Inorganic Chemistry

Article

pubs.acs.org/IC

Synthesis, Structure, and Properties of a Series of Chiral Tweezer–Diamine Complexes Consisting of an Achiral Zinc(II) Bisporphyrin Host and Chiral Diamine Guest: Induction and Rationalization of Supramolecular Chirality

Sanfaori Brahma, Sk Asif Ikbal, and Sankar Prasad Rath*

Department of Chemistry, Indian Institute of Technology Kanpur, Kanpur-208016, India

Supporting Information

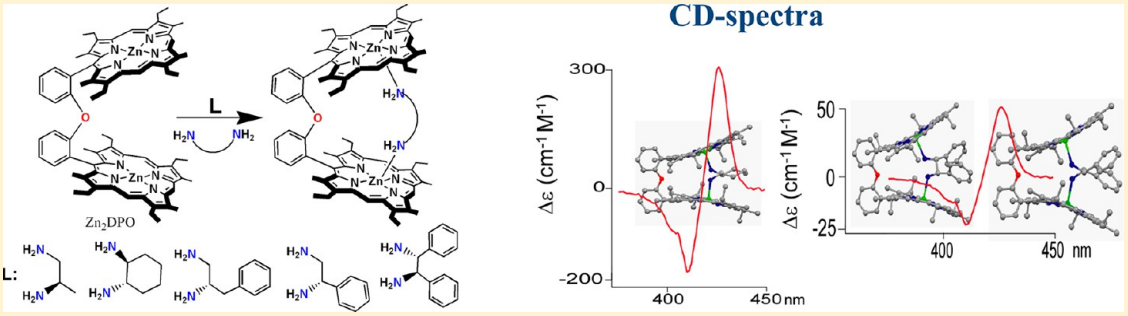

ABSTRACT: We report here the synthesis, structure, and spectroscopic properties of a series of supramolecular chiral 1:1 tweezer–diamine complexes consisting of an achiral Zn(II) bisporphyrin (Zn_2DPO) host and five different chiral diamine guests, namely, (*R*)-diaminopropane (DAP), (1*S*,2*S*)-diaminocyclohexane (CHDA), (*S*)-phenylpropane diamine (PPDA), (*S*)-phenyl ethylenediamine (PEDA), and (1*R*,2*R*)-diphenylethylene diamine (DPEA). The solid-state structures are preserved in solution, as reflected in their ^{1}H NMR spectra, which also revealed the remarkably large upfield shifts of the N*H*$_2$ guest protons with the order Zn_2DPO·DAP > Zn_2DPO·CHDA > Zn_2DPO·PPDA> Zn_2DPO·PEDA ≫ Zn_2DPO·DPEA, which happens to be the order of binding constants of the respective diamines with Zn_2DPO. As the bulk of the substituent at the chiral center of the guest ligand increases, the Zn–N_{ax} distance of the tweezer–diamine complex also increases, which eventually lowers the binding of the guest ligand toward the host. Also, the angle between the two porphyrin rings gradually increases with increasing bulk of the guest in order to accommodate the guest within the bisporphyrin cavity with minimal steric clash. The notably high amplitude bisignate CD signal response by Zn_2DPO·DAP, Zn_2DPO·CHDA, and Zn_2DPO·PPDA can be ascribed to the complex's high stability and the formation of a unidirectional screw as observed in the X-ray structures of the complexes. A relatively lower value of CD amplitude shown by Zn_2DPO·PEDA is due to the lower stability of the complex. The projection of the diamine binding sites of the chiral guest would make the two porphyrin macrocycles oriented in either a clockwise or anticlockwise direction in order to minimize host–guest steric clash. In sharp contrast, Zn_2DPO·DPEA shows a very low amplitude bisignate CD signal due to the presence of both left- (dictated by the pre-existing chirality of (1*R*,2*R*)-DPEA) and right-handed screws (dictated by the steric differentiation at the chiral center) of the molecule, as evident from X-ray crystallography. The present work demonstrates a full and unambiguous rationalization of the observed chirality transfer processes from the chiral guest to the achiral host.

INTRODUCTION

Supramolecular chirogenesis is one of the most important interdisciplinary fields to be looked into, because of its occurrences in many natural (DNA double helix, heme proteins, secondary α-helix structure of proteins, etc.) and artificial systems.[1] Therefore, it is very important to have clear insight into the various factors that control the processes of chirality transfer, which will help in developing more advanced knowledge about the subject that will promote not only the understanding of the fundamental science but also its applicability in different areas of science. Porphyrinoids have been shown to be well suited for studying the events involved in the supramolecular chirality induction mainly due to their interesting photophysical properties and possibility of versatile modification of the porphyrin at their periphery or by metalations of the porphyrin core.[1−16] As noncovalent interactions are the key elements of supramolecular chemistry, various external (such as temperature, polarity and viscosity of the solvent) and internal (such as bond strength, stoichiometry, steric and conformational freedom of the complex) factors that control the chirality induction process would need extensive investigations. Upon formation of a chiral host–guest supramolecular complex between an achiral bis-metalloporphyrin

Received: May 2, 2013
Published: November 25, 2013

derivative and a chiral guest, a bisignate CD curve (so-called exciton couplet) is observed, with two bands of opposite sign and similar intensity in the porphyrin spectral region, which is diagnostic of the guest's absolute configuration.[2] However, in the case of chiral assemblies consisting of more than one porphyrin, the dynamic nature of noncovalent assemblies and the complex electronic structure of the pigments as a consequence of its several possible orientations are the two major factors that make such a study difficult.[2]

Studies on the supramolecular chirality induction in Zn(II) bisporphyrins upon coordination with chiral guest ligands are amply documented.[1−13] Upon formation of a 1:1 host−guest sandwich complex through the ditopic binding of the bidentate chiral guest to the porphyrin metal centers, chirality is transferred from the chiral guest to the host due to the generation of a preferential chiral twist in the porphyrin−porphyrin arrangement, producing an exciton-coupled CD response.[2] The sign of the Soret CD couplet is dictated by the direction of interporphyrin helical twist, while its intensity depends on several other factors.

Bis(zinc octaethylporphyrin) serves as an effective achiral host molecule to form a chiral 1:1 sandwich complex upon interaction with an enantiopure bidentate guest, (1*R*,2*R*)-cyclohexane diamine, which has shown a very high amplitude bisignate CD signal (−590 M^{-1} cm^{-1}).[3a] The X-ray structure and the spectroscopic data of the complex have been utilized to rationalize the observed sign and amplitude of the CD signal.[3a] There are, however, many 1:1 host−guest complexes reported in the literature in which CD amplitudes are much less[2,3] and also the sign of the "predicted" CD signal is opposite the experimental observations.[7b,e] Thus a comprehensive understanding of the underpinning mechanisms and various influencing factors responsible for the supramolecular chirality induction phenomena would be extremely important. We report here the synthesis, structure, and spectroscopic properties of a series of supramolecular chiral tweezer−diamine complexes consisting of an achiral diphenyl ether-bridged Zn(II) bisporphyrin host and variety of chiral diamine guests, which, however, provide very rare examples of explicit crystallographic characterization of the chiral host−guest complexes. The bulk of the substituent at the stereogenic center has been varied successively in the present investigation in order to specify the role played by the preorganization of the guest binding sites as well as the steric differentiation at the chiral center in the overall helicity of the complexed porphyrin tweezers. This also provides a unique opportunity to observe the transitions where the steric differentiation at the stereogenic center dominates over the preorganized projection of the guest binding sites and *vice versa*. Crystallographic and other spectroscopic investigation of the complexes enable us to rationalize the origin of the optical activity unambiguously in the supramolecular host−guest complexes at the molecular level. The present investigation will also allow comparing and correlating the chirality induction process with the nature of the supramolecular host for absolute stereochemical determination. These systematic studies will help in designing efficient chirality sensor for numerous classes of chiral molecules and will create clear perspective for the building of smart chiroptical devices. We have recently reported briefly the X-ray structure and properties of two such complexes as a preliminary communication.[4]

RESULTS AND DISCUSSION

Diphenyl ether-bridged Zn(II) bisporphyrin, Zn_2DPO, is prepared using the procedure reported previously.[17] Interaction of the chiral diamine ligands with Zn_2DPO has been monitored by UV−visible spectroscopy. Addition of enantiomerically pure (*R*)-diaminopropane, (*R*)-DAP, to the chloroform solution of Zn_2DPO at room temperature results in a large red shift of the Soret (393 to 412 nm) and Q-bands (536 to 547 nm, 571 to 581 nm) due to the formation of the 1:1 sandwich complex Zn_2DPO·DAP in solution. The spectral pattern does not change any more even at a very high concentration of (*R*)-DAP, which suggests the complex is very stable in the 1:1 sandwich form. Figure 1 demonstrates the spectral changes of

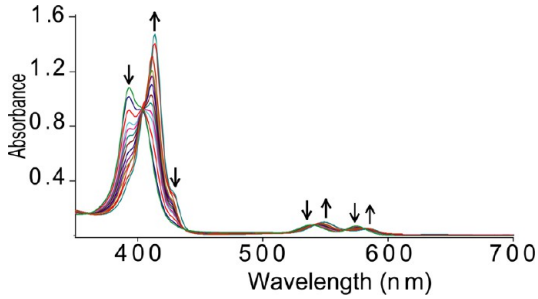

Figure 1. UV−visible spectral changes of Zn_2DPO in chloroform upon addition of (*R*)-diaminopropane as the host:guest molar ratio changes from 1:0 to 1:245 at 295 K.

Zn_2DPO in chloroform upon gradual addition of (*R*)-DAP, which eventually produces the tweezer−diamine complex Zn_2DPO·DAP in solution. The Soret band at 412 nm and shoulder at 426 nm arise because of exciton interactions of high-energy (in-phase) and low-energy (out-of-phase) transition dipole moments, respectively,[2b] of the two cofacial porphyrin units, which is in line with Kasha's exciton coupling theory.[18]

Similar spectral changes are also observed when enantiomerically pure (1*S*,2*S*)-diaminocyclohexane, (1*S*,2*S*)-CHDA, (*S*)-phenylpropane diamine, (*S*)-PPDA, (*S*)-phenyl ethylenediamine, (*S*)-PEDA, and (1*R*,2*R*)-diphenylethylene diamine, (1*R*,2*R*)-DPEA, are used as guest molecules to form Zn_2DPO·CHDA, Zn_2DPO·PPDA, Zn_2DPO·PEDA, and Zn_2DPO·DPEA, respectively. All the complexes have been isolated as crystalline solid in good yields and structurally characterized. However, there is no evidence of formation of 1:2 host−guest complexes even at very high concentration of ligand.[3,4] Scheme 1 shows the synthetic outline of all the complexes reported here along with their abbreviations used in the present investigation, while the synthetic procedures and their spectral characterizations are given in the Experimental Section.

Job's continuous variation plot is very helpful in determining the stoichiometry of the complex formation in solution. Figures S1 demonstrates the plot for all five complexes Zn_2DPO·DAP, Zn_2DPO·CHDA, Zn_2DPO·PPDA, Zn_2DPO·PEDA, and Zn_2DPO·DPEA, which shows that the complexes are optimally formed at equimolar concentration of the Zn(II) bisporphyrin host and chiral diamine guest (i.e., 0.5 mol fraction) and thus confirming the formation of a 1:1 sandwich complex.

Crystallographic Characterization. Dark purple crystals of Zn_2DPO·DAP were grown via slow diffusion of *n*-hexane into dichloromethane solution of the complex at room

dx.doi.org/10.1021/ic401091r | *Inorg. Chem.* 2014, 53, 49−62

Scheme 1

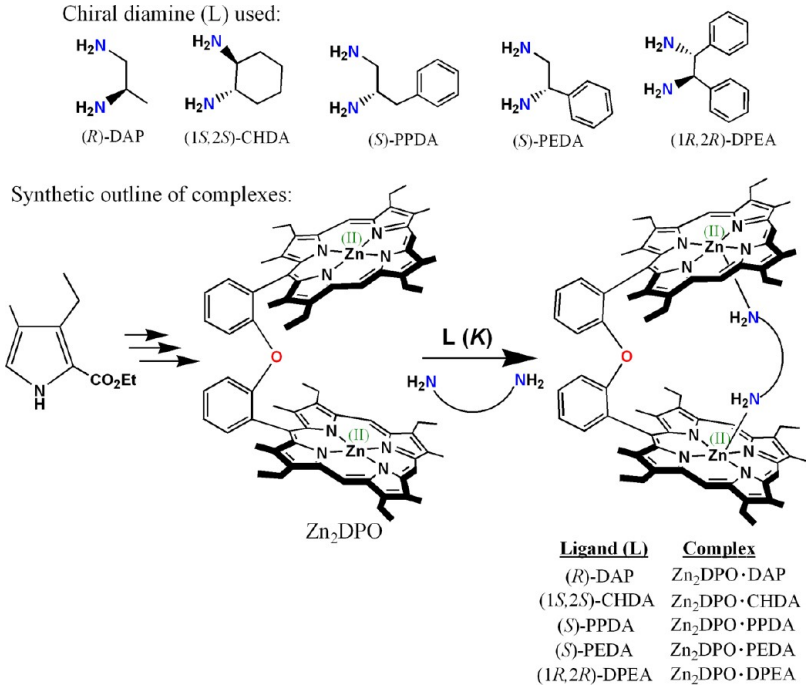

temperature in air. The complex crystallizes in the monoclinic crystal system in the *C*2 chiral space group; a perspective view is depicted in Figure 2. Two amino groups of DAP are

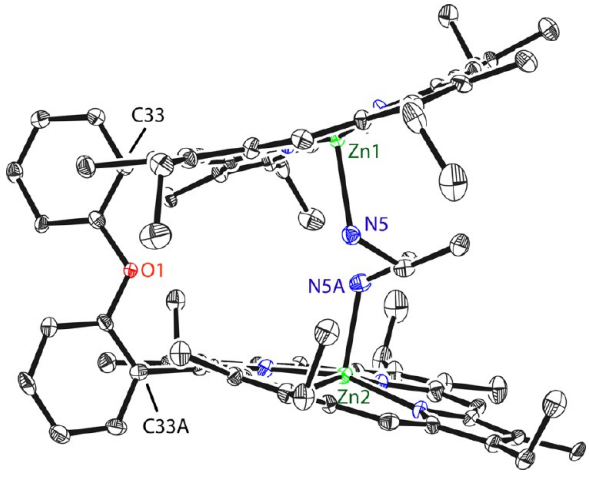

Figure 2. Perspective view of $Zn_2DPO·DAP$ showing 50% thermal contours for all non-hydrogen atoms at 100 K (H atoms have been omitted for clarity).

coordinated to Zn atoms of Zn_2DPO, forming a 1:1 host–guest complex in which two porphyrin planes make a dihedral angle of 28.6°. The Zn centers of two porphyrin units in $Zn_2DPO·DAP$ are separated by 5.99 Å and have five-coordinated square-pyramidal geometry in which the metal ions are displaced by 0.34 and 0.35 Å from the least-squares plane of the $C_{20}N_4$ porphyrinato core for core I and core II, respectively. Two spatially orientated $Zn–N_{ax}$ coordination bonds arising from the projection of the amino coordinating site attached to the stereocenter of the (*R*)-DAP ligand direct two porphyrin rings to be oriented in a unidirectional screw arrangement in order to minimize the host–guest steric interactions, which eventually transfer the chirality informations from the enantiomeric guest to the achiral host in the supramolecular complex. The porphyrin rings are twisted anticlockwise relative to each other around the diphenyl ether bridge with a torsional angle Φ (Zn1–C33–C33A–Zn2) of −33.4(5)°. Molecular packing in the crystal lattice is shown in Figure 3.

$Zn_2DPO·CHDA$ crystallizes by slow diffusion of *n*-hexane into a solution of the complex in chloroform at room temperature in air to give a monoclinic crystal system with the $P2_1$ chiral space group. There are two molecules in the asymmetric unit, which are also different structurally;

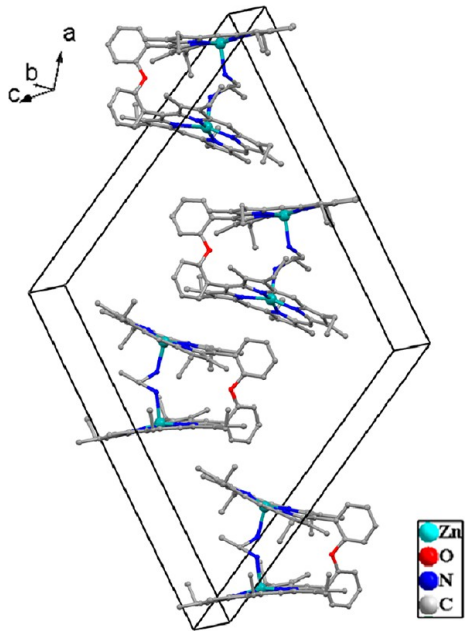

Figure 3. Diagram illustrating the packing of $Zn_2DPO·DAP$ in the unit cell (H atoms have been omitted for clarity).

dx.doi.org/10.1021/ic401091r | *Inorg. Chem.* 2014, 53, 49–62

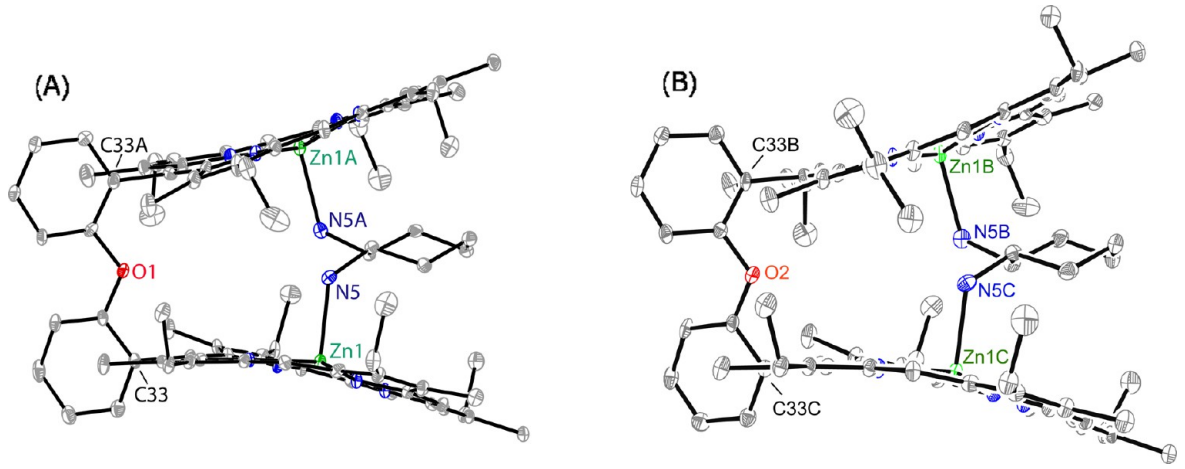

Figure 4. Perspective views of Zn_2DPO·CHDA of (A) molecule I and (B) molecule II showing 50% thermal contours for all non-hydrogen atoms at 100 K (H atoms have been omitted for clarity).

perspective views are shown in Figure 4. From the crystal structure of Zn_2DPO·CHDA, it can be seen that Zn_2DPO holds the ligand inside its cavity through the ditopic binding of two equatorially oriented amino substituents of the ligand moiety to the Zn centers. Two porphyrin units of Zn_2DPO·CHDA open up its jaw to accommodate the CHDA ligand inside its cavity, which make dihedral angles of 28.7° and 30.8° between the two porphyrin rings for molecules I and II, respectively. The Zn center is in a five-coordinate square-pyramidal geometry, and the nonbonding Zn···Zn distances are 5.91 and 5.87 Å, respectively, for molecules I and II. For molecule I, the Zn atoms are displaced by ∼0.36 Å from the mean porphyrin planes, while displacements of 0.37 Å are observed for molecule II. The cyclohexane ring of CHDA is in a chair conformation and lies parallel to the two porphyrin rings, thus allowing attractive CH−π interactions between the ligand and porphyrin moieties, which further stabilize the host−guest complexation. Most significantly, projection of the binding sites of the ligand moiety from the chiral center compel the two porphyrin rings to have a stereospecific orientation in order to minimize the host−guest steric interactions. The induction of asymmetry information of the enantiomerically pure chiral ligand to the achiral host is highly anticipated from the unidirectional screw observed in the bisporphyrin moiety. The porphyrin rings are twisted clockwise around the diphenyl ether bridge, with torsional angles Φ (Zn1−C33−C33A−Zn1A) of +30.9(5)° and +30.8(5)° for molecules I and II, respectively. Molecular packing of the complex in the crystal lattice is shown in Figure 5.

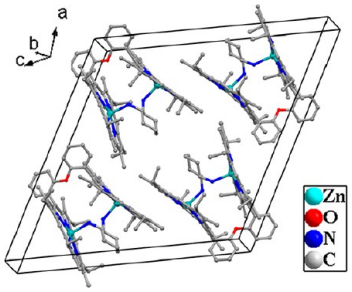

Figure 5. Diagram illustrating the packing of Zn_2DPO·CHDA in the unit cell. H atoms have been omitted for clarity.

Dark purple crystals of Zn_2DPO·PPDA were deposited in high yields by slow diffusion of acetonitrile into the dichloromethane solution of the complex at room temperature in air. The complex crystallizes in the monoclinic crystal system with the *C*2 chiral space group; a perspective view is shown in Figure 6. Chiral (*S*)-PPDA is coordinated to the Zn atoms of

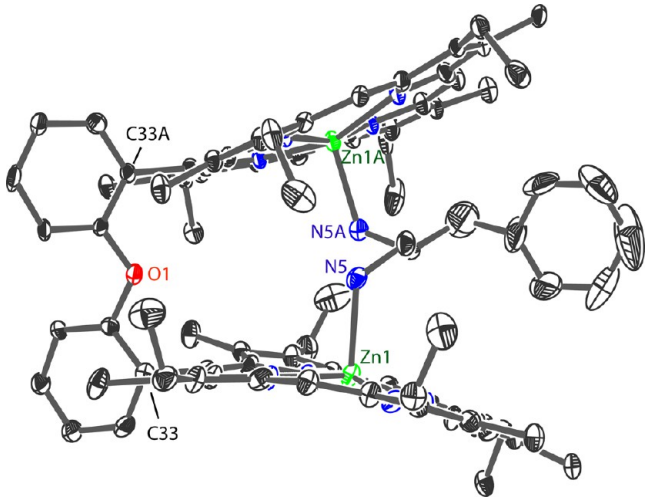

Figure 6. Perspective view of Zn_2DPO·PPDA showing 50% thermal contours for all non-hydrogen atoms at 100 K (H atoms have been omitted for clarity).

the two porphyrin units of Zn_2DPO through the amino binding sites, yielding a supramolecular 1:1 sandwich complex with a dihedral angle of 32.5° defined by the mean porphyrin planes ($C_{20}N_4$ porphyrinato core). The Zn centers of the two porphyrin units in a molecule are separated by a distance of 5.99 Å and are displaced by 0.39 Å from the least-squares plane of the $C_{20}N_4$ porphyrinato core. The projection of the two amino coordinating sites of the PPDA ligand direct two porphyrin rings to produce unidirectional screw with a torsional angle Φ (Zn1−C33−C33A−Zn1A) of +32.7(5)° in order to minimize the host−guest steric interactions. A diagram illustrating the molecular packing in the crystal lattice is shown in Figure 7.

Crystals of Zn_2DPO·PEDA have been obtained via slow diffusion of acetonitrile to the dichloromethane solution of the

dx.doi.org/10.1021/ic401091r | *Inorg. Chem.* 2014, 53, 49−62

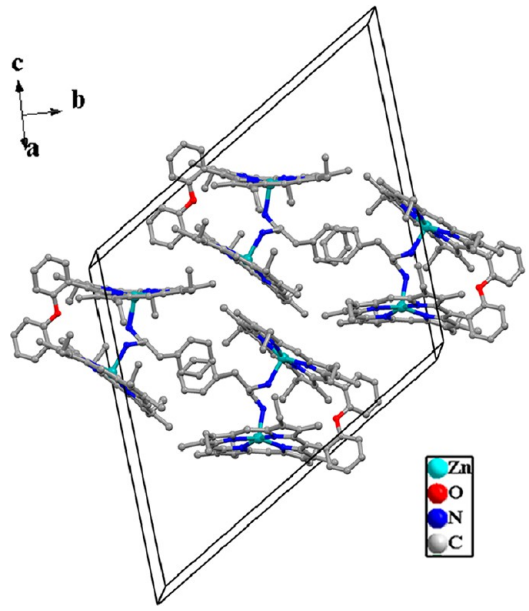

Figure 7. Diagram illustrating the packing of Zn_2DPO·PPDA in the unit cell (H atoms have been omitted for clarity).

complex in air at room temperature, and one such crystal was used for X-ray structure determination. The molecule crystallizes in the monoclinic crystal system with the *C*2 chiral space group. A perspective view of the crystal structure is illustrated in Figure 8. The coordinating $-NH_2$ sites of the

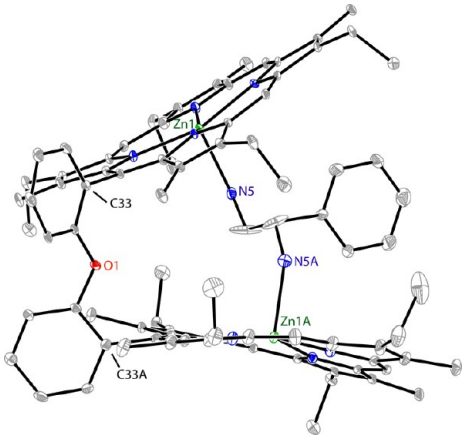

Figure 8. Perspective view of Zn_2DPO·PEDA showing 50% thermal contours for all non-hydrogen atoms at 100 K (H atoms have been omitted for clarity).

chiral (*S*)-PEDA bind to the zinc centers of Zn_2DPO to produce a 1:1 sandwich complex with a dihedral angle of 39.5° defined by two mean porphyrin planes. Zn centers are displaced by ~0.32 Å from the mean porphyrin plane with a nonbonding Zn···Zn distance of 6.72 Å. It is interesting to note that the two $Zn-N_{ax}$ distances are different in the molecule: the longer distance involves the nitrogen that is closer to the bulky phenyl group. The phenyl group of the PEDA ligand lies perpendicular to the porphyrin rings, which facilitates the attractive CH–π interactions with the porphyrin rings and, thus, brings some stability for the complex. The coordination of the preorganized amino binding sites of the chiral ligand leads to the formation of unidirectional screw with a torsional angle Φ (Zn1–C33–C33A–Zn1A) of +35.2(5)°. A diagram illustrating the molecular packing in the crystal lattice is shown in Figure 9.

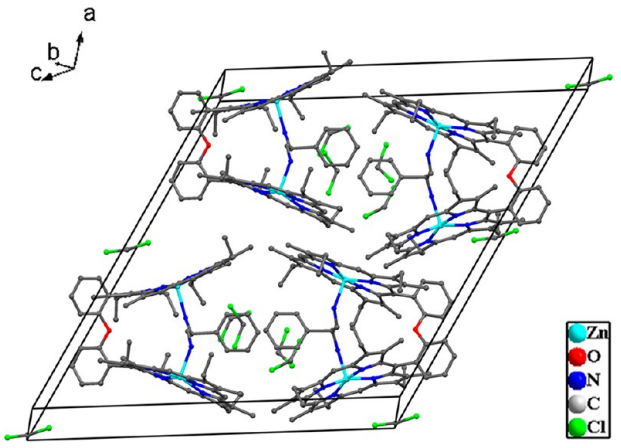

Figure 9. Diagram illustrating the packing of Zn_2DPO·PEDA·$5CH_2Cl_2$ in the unit cell. H atoms have been omitted for clarity.

Slow diffusion of *n*-hexane into a chloroform solution of the molecule at room temperature gave dark purple crystals, from which an appropriate crystal was chosen for X-ray diffraction experiments. The molecule crystallizes in the monoclinic crystal system in the *C*2 chiral space group; a perspective view is shown in Figure 10. There are two molecules in the asymmetric unit with very different structural and geometrical parameters. Each Zn center is in square-pyramidal geometry, where the metals are displaced by 0.36 and 0.43 Å for molecules I and II, respectively, from the mean porphyrin planes. The bulky phenyl substituents in DPEA generate significant steric

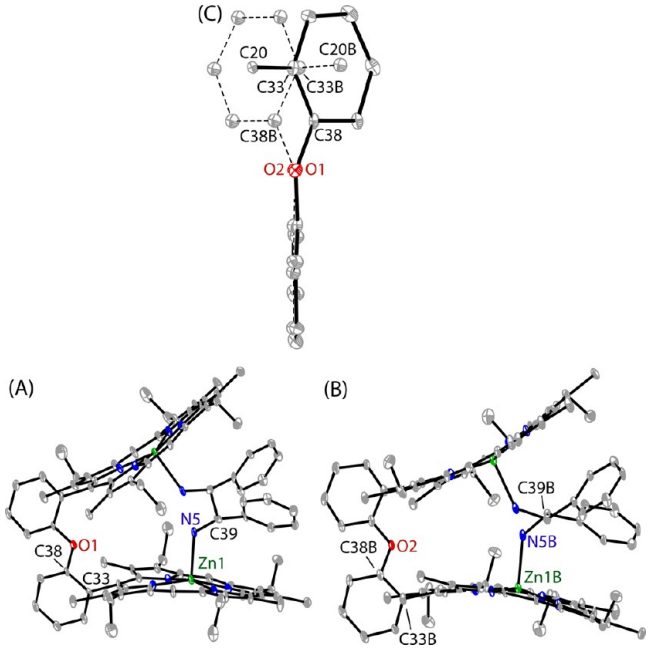

Figure 10. Perspective views of Zn_2DPO·DPEA of (A) molecule I and (B) molecule II showing 50% thermal contours for all non-hydrogen atoms at 100 K (H atoms and uncoordinated solvent molecule $CHCl_3$ have been omitted for clarity). (C) Overlay of the diphenyl ether bridge between two molecules in Zn_2DPO·DPEA, which also displays the projection of the porphyrin *meso* carbons that are bridged.

dx.doi.org/10.1021/ic401091r | *Inorg. Chem.* 2014, 53, 49–62

interactions in the 1:1 sandwich complex, which results in a significant increase in the interporphyrin angle to 40.3° and 38.7° for molecules I and II, respectively. Zn···Zn separations also have increased significantly in order to minimize the nonbonding contacts within the supramolecular host–guest complex and thus leads to the weaker binding of the DPEA ligand in Zn_2DPO·DPEA (*vide infra*). As a result, the average Zn–N_{ax} distance is longer in Zn_2DPO·DPEA as compared to the similar distance observed in Zn_2DPO·DAP, Zn_2DPO·CHDA, and Zn_2DPO·PPDA. The nonbonding Zn···Zn distances are found to be very different between the two molecules: 6.37 Å for molecule I and 5.88 Å for molecule II. Interestingly, the two zinc porphyrin units are twisted clockwise and anticlockwise around the bridging ligand, with a torsional angle Φ (Zn1–C33–C33A–Zn1A) of +34.5(7)° and −33.1(7)° for molecules I and II, respectively. According to the projection of the ligand's two amino groups, there could have been unidirectional molecules of left-handed screw sense only; however, the molecule with right-handed screw sense are also apparent, as evident in the X-ray crystallography. Molecular packing in the crystal lattice is demonstrated in Figure 11. The selected bond distances and angle are given in Table S1, while data collection parameters for all the 1:1 complexes are listed in Table S2.

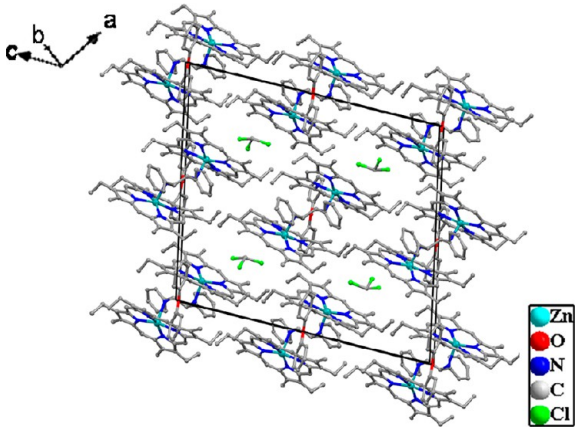

Figure 11. Diagram illustrating the packing of Zn_2DPO·DPEA·$CHCl_3$ in the unit cell. H atoms have been omitted for clarity.

The salient structural features of the 1:1 complexes consisting of the chiral diamine guests and Zn(II) bisporphyrin host reported here and the lone structurally characterized chiral tweezer–diamine reported in the literature are compared in Table 1. Among the host–guest complexes reported here with Zn_2DPO, an increase in the size of the substituent at the chiral diamine guest results in an increase of Zn–N_{ax} distance. Also, the angle between the two porphyrin rings and the average displacement of atoms from the mean porphyrin plane gradually increases with the increase in the bulk of the substituent at the diamine ligand in order to accommodate the guest within the bisporphyrin cavity with minimum steric host–guest clash. A diagram illustrating the bulk of the chiral guest ligand within the bisporphyrin cavity is shown in Figure S2. For Zn_2DPO·DAP, Zn_2DPO·PPDA, Zn_2DPO·PEDA, and Zn_2(ethane-bridged bisporphyrin)·CHDA, there is only one molecule in the asymmetric unit, while in Zn_2DPO·CHDA and Zn_2DPO·DPEA, there are two molecules and each is present in the asymmetric unit. However, only in Zn_2DPO·DPEA are very different structural and geometrical parameters observed between the two molecules due to the presence of bulky phenyl substituents in DPEA guest ligand. For molecule I, the Zn–N_p distance is shortest in the series, while the Zn···Zn nonbonding distance is much longer than that of molecule II. For molecule II, the Zn–N_{ax} distance is remarkably longer than that of molecule I. In both Zn_2DPO·PEDA and Zn_2DPO·DPEA, there are bulky phenyl substituents at the chiral center of the guest ligand, which, however, produces large steric interaction with the porphyrin rings. The effect can be seen just by looking at two Zn–N_{ax} distances of 2.189(4) and 2.247(4) Å observed in Zn_2DPO·PEDA: the $-NH_2$ group nearer to the phenyl group binds weaker compared to the distant $-NH_2$. It is also interesting to note in Zn_2DPO·DPEA that two zinc porphyrin rings twisted in a clockwise direction around the diphenyl ether bridge in molecule I, while they rotate in the anticlockwise direction in molecule II. In sharp contrast, the two molecules that are present in the asymmetric unit in Zn_2DPO·CHDA are very similar and, in both molecules, two zinc porphyrins are twisted only in a clockwise direction around the diphenyl ether bridge with a torsional angle of +30.9(5)° and +30.8(5)°, respectively.

It would be interesting to compare the binding of 1,2-diaminocyclohexane (CHDA) with Zn_2DPO reported here and also with ethane-bridged Zn(II) bisporphyrin reported earlier.[3a] While the average Zn–N_p distance is similar for both molecules, the Zn–N_{ax} distances are relatively shorter in the latter complex. Also, several geometrical parameters such as displacement of the metal from the mean porphyrin plane, the dihedral angle between the two porphyrin planes, and the torsional angles are higher in the latter complex with a lesser value of Zn···Zn separation. Two oppositely oriented amino groups in CHDA result in the exclusive formation of a 1:1 complex with a binding constant of 1.60×10^5 M^{-1} (*vide infra*) with Zn_2DPO and 1.25×10^7 M^{-1} with ethane-bridged Zn(II) bisporphyrin. Thus, CHDA binds strongly with a highly flexible ethane-bridged bisporphyrin, which results in a very large torsional angle of −54.1°.[3a]

^{1}H NMR. The formation of 1:1 complexes in solution between the Zn_2DPO host and all five chiral diamines is also established by the ^{1}H NMR spectra. Figure 12 shows the relevant spectra coming from the reaction between Zn_2DPO and (*R*)-diaminopropane. Trace A shows the well-resolved spectrum of Zn_2DPO in $CDCl_3$, while trace B shows the ^{1}H NMR spectra of the crystalline sample of Zn_2DPO·DAP dissolved in the same solvent. Trace C, however, shows the ^{1}H NMR spectrum of the free (*R*)-DAP alone under identical conditions. As can be seen, the ^{1}H NMR spectrum of Zn_2DPO·DAP (trace B) shows a large change from that of Zn_2DPO and the free (*R*)-DAP ligand. The identical 10- and 20-*meso* protons are noticeably downfield shifted by $\Delta\delta$ = 1.85 and 0.78 ppm, respectively, due to conformational changes upon 1:1 complexation, which results in moving the two porphyrin rings further apart from each other. These protons, also, become nonequivalent as a result of their different exposure to the ring current effect due to the twisting of the two porphyrin subunits in solution, which were otherwise identical. However, the 15-*meso* proton is upfield shifted by $\Delta\delta$ = 0.62 ppm. The most interesting feature is the remarkably large upfield shifts of the guest ligand protons H^3 ($\Delta\delta$ = 9.33 ppm), NH_2 ($\Delta\delta$ = 9.52 and 9.40 ppm), H^2 ($\Delta\delta$ = 9.04 ppm), H^1 ($\Delta\delta$ = 8.2 ppm), and CH_3(L) ($\Delta\delta$ = 5.65 ppm) as the ligand emerges within the porphyrin ring current. The order of the shifts, as observed here

dx.doi.org/10.1021/ic401091r | *Inorg. Chem.* 2014, 53, 49–62

Table 1. Selected Structural Parameters of Tweezer−Diamine Complexes

complex			Zn−N_p[a]	Zn−N_{ax}[a]	Δ^{Zn}_{24}[b]	Δ_{24}[c]	Zn···Zn[d]	θ[e]	α[f]	lateral shift[g]	torsion angle (Φ)[h]
Zn_2DPO·DAP		core I	2.070(4)	2.191(4)	0.34	0.16	5.992(2)	28.6	25.1	2.80	−33.4 (5)
		core II	2.070(4)	2.177(4)	0.35	0.12					
Zn_2DPO·CHDA	molecule I	core I	2.073(4)	2.197(5)	0.37	0.16	5.908(2)	28.7	23.7	2.64	30.9(5)
		core II	2.069(4)	2.213(5)	0.35	0.12					
	molecule II	core I	2.057(4)	2.214(5)	0.35	0.16	5.872(2)	30.8	24.6	2.72	30.8(5)
		core II	2.077(4)	2.178(4)	0.39	0.14					
Zn_2DPO·PPDA		core I	2.070(6)	2.223(6)	0.38	0.18	5.989(2)	32.5	25.9	2.94	32.7(5)
		core II	2.078(6)	2.184(6)	0.41	0.14					
Zn_2DPO·PEDA		core I	2.073(4)	2.189(4)	0.32	0.13	6.724(2)	39.5	28.0	3.43	35.2(5)
		core II	2.060(4)	2.247(4)	0.33	0.16					
Zn_2DPO·DPEA	molecule I		2.053(8)	2.209(8)	0.36	0.16	6.372(3)	40.3	29.0	3.39	34.5(7)
	molecule II		2.073(8)	2.232(8)	0.43	0.18	5.879(3)	38.7	26.9	3.01	−33.1(7)
Zn_2bisporphyrin·CHDA[i]		core I	2.079	2.170	0.47	0.11	5.604(5)	39.5	29.1	3.08	−54.1(5)
		core II	2.073	2.186	0.40	0.10					

[a]Average value in Å. [b]Displacement (in Å) of Zn from the least-squares plane of the $C_{20}N_4$ porphyrinato core. [c]Average displacement (in Å) of atoms from the least-squares plane of the $C_{20}N_4$ porphyrinato core. [d]Nonbonding distance in Å. [e]Angle between two least-squares plane of the $C_{20}N_4$ porphyrinato core. [f]Slip angle in degrees (slip angles were calculated as the average angle between the vector joining the two macrocyclic centers and the unit vectors normal to the two macrocyclic centers of the $C_{20}N_4$ porphyrinato core). [g]Lateral shift (in Å) is defined as [sin(α) × (Ct···Ct distance)]. [h]Torsional angle (Zn1−C33−C33A−Zn1A). [i]Taken from ref 3a.

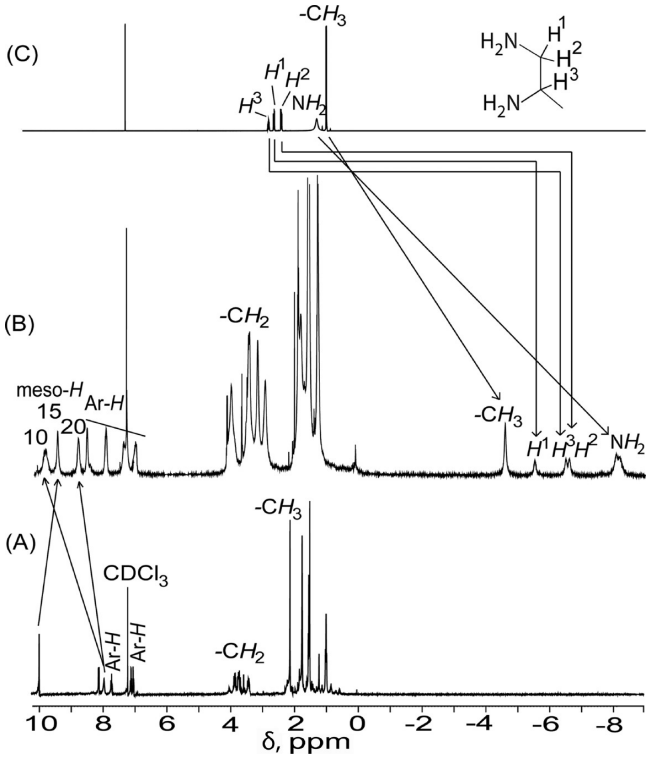

Figure 12. ^{1}H NMR spectra of (A) Zn_2DPO, (B) Zn_2DPO·DAP, and (C) (*R*)-DAP at 295 K in $CDCl_3$. Inset shows the proton numbering scheme of (*R*)-DAP. Porphyrin numbering scheme is shown in Scheme S1 in the Supporting Information.

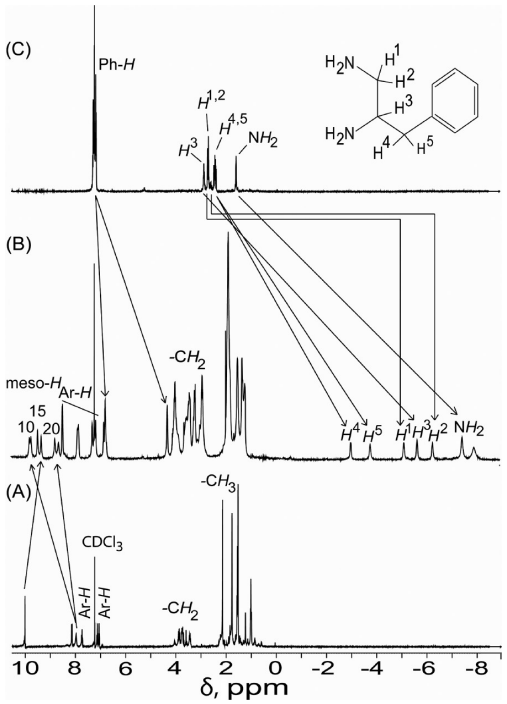

Figure 13. ^{1}H NMR spectra of (A) Zn_2DPO, (B) Zn_2DPO·PPDA, and (C) (*S*)-PPDA at 295 K in $CDCl_3$. Inset shows the proton numbering scheme of (*S*)-PPDA. Porphyrin numbering scheme is shown in Scheme S1 in the Supporting Information.

in trace B, correlates well with the geometry of the 1:1 sandwich complex and the close proximity of the guest protons to the porphyrin planes.

Similar shifts of the guest's proton clamped between two porphyrin subunits have also been observed from the ^{1}H NMR spectrum of the crystalline sample of Zn_2DPO·PPDA in $CDCl_3$ as depicted in Figure 13. Because of the encapsulation of the guest ligand inside the porphyrin cavity, all the guest protons get upfield-shifted in the ^{1}H NMR spectrum of the complex. The H^2 proton is shifted by 9.12 ppm from its resonance in the absence of Zn(II) bisporphyrin, while two NH_2 protons are shifted by 9.70 and 9.22 ppm. However, the protons of the phenyl ring of the ligand are less upfield shifted because the phenyl group is directed to the outside of the bisporphyrin cavity. The shifting of *ortho*, *meta*, and *para* protons is, respectively, 2.90, 0.41, and 0.35 ppm. The identical 10- and 20-*meso* protons of the Zn_2DPO host produce four nonidentical peaks because of complexation with the asymmetrical chiral PPDA ligand. There also appear two resonances for 15-*meso* protons for the same reason.

dx.doi.org/10.1021/ic401091r | *Inorg. Chem.* 2014, 53, 49−62

Figure 14 compares the ^{1}H NMR of Zn_2DPO, Zn_2DPO·PEDA, and (*S*)-PEDA in $CDCl_3$. As observed in other

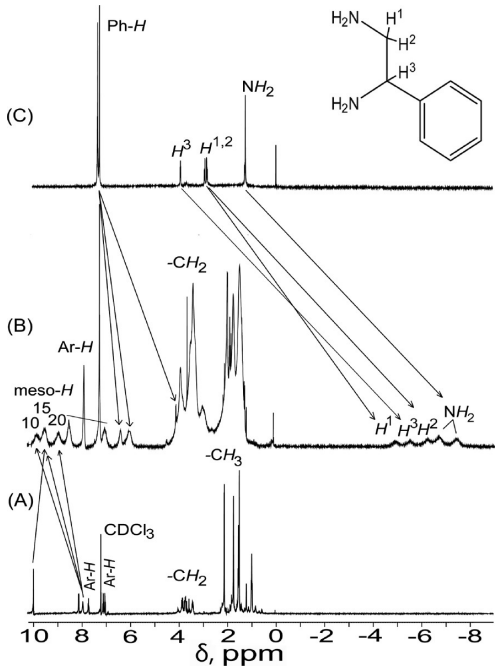

Figure 14. ^{1}H NMR spectra of (A) Zn_2DPO, (B) Zn_2DPO·PEDA, and (C) (*R*)-PEDA at 295 K in $CDCl_3$. Inset shows the proton numbering scheme of (*S*)-PEDA. Porphyrin numbering scheme is shown in Scheme S1 in the Supporting Information.

tweezer−diamine complexes reported here, the ligand protons of the 1:1 sandwich complex Zn_2DPO·PEDA are also acquainted with a similar shifting, H^3 ($\Delta\delta$ = 9.49 ppm) and NH_2 ($\Delta\delta$ = 8.02 and 8.72 ppm). However, three broad *meso* signals are observed for the complex instead of six distinct *meso* proton signals that are expected due to the asymmetric nature of the guest ligand. Figures S3 and S4, respectively, demonstrate the ^{1}H NMR spectra of Zn_2DPO·CHDA and Zn_2DPO·DPEA, in which a similar shift of the guest protons is observed. Zn_2DPO·CHDA shows remarkably large upfield shifts of the ligand protons (for H^5, $\Delta\delta$ = 9.33 ppm and for NH_2, $\Delta\delta$ = 9.62 ppm). However, because of the lower binding affinity of (1*R*,2*R*)-DPEA toward Zn_2DPO (*vide infra*), Zn_2DPO·DPEA shows very broad signals. Complete assignments of the resonances for all the complexes reported here have been made on the basis of relative intensities of the signals and ^{1}H−^{1}H COSY, as demonstrated in Figures S5−S7 for Zn_2DPO·CHDA, Zn_2DPO·DAP, and Zn_2DPO·PPDA, respectively. The spectral patterns observed in the present investigation are also similar to other 1:1 complexes reported in the literature.[2,3,5−7]

It would be appropriate to compare now the ^{1}H NMR spectra of all five chiral complexes reported here, which have been demonstrated in Figure 15. The spectral pattern looks very similar; guest protons are all upfield shifted, in which NH_2 protons are shifted most followed by other protons. It is found that the largest upfield shifts of the NH_2 protons follow the order Zn_2DPO·DAP > Zn_2DPO·CHDA > Zn_2DPO·PPDA > Zn_2DPO·PEDA ≫ Zn_2DPO·DPEA, which happens to be the order of binding constants of the respective guest ligands toward Zn_2DPO (*vide infra*). *Meso* proton signals become nonequivalent as a result of twisting of the bisporphyrin

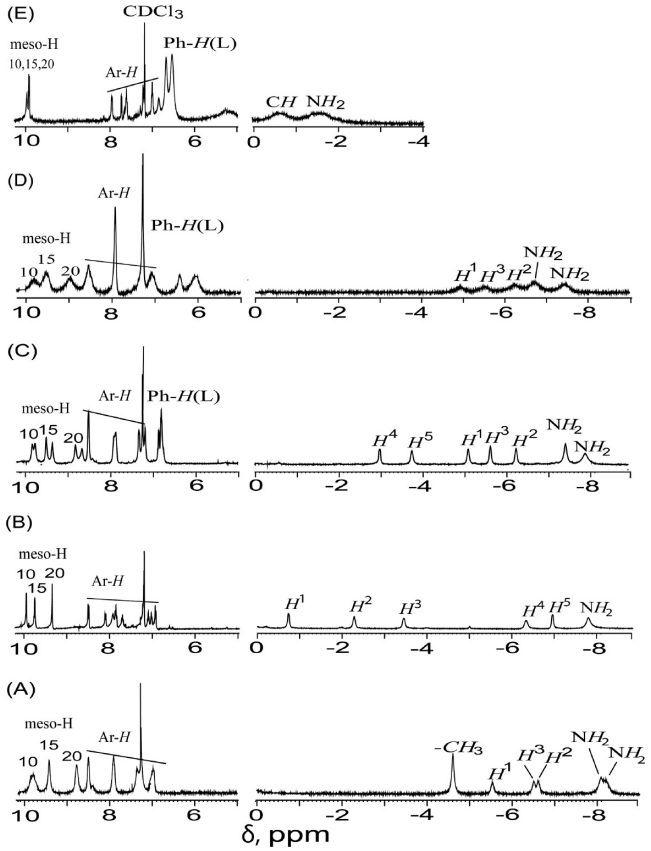

Figure 15. ^{1}H NMR spectra in $CDCl_3$ at 295 K for (A) Zn_2DPO·DAP, (B) Zn_2DPO·CHDA, (C) Zn_2DPO·PPDA, (D) Zn_2DPO·PEDA, and (E) Zn_2DPO·DPEA.

framework along the diphenyl ether bridge in the complex. Six *meso* signals are clearly visible for Zn_2DPO·PPDA because of the asymmetric nature of the PPDA guest ligand. However, instead of six *meso* signals expected for other asymmetric ligands (DAP and PEDA) used in the present investigation, three broad *meso* peaks are observed in the complex. It is also interesting to note that while other complexes showed well-resolved signals particularly for guest and *meso* protons, Zn_2DPO·DPEA depicts very broad ^{1}H NMR resonances. Also the upfield shifting of the diphenylethylene diamine protons in the tweezer−diamine complex is much less compared to others. This is due to weaker binding of DPEA with Zn_2DPO along with the presence of two structurally different molecules in solution, which produces average signals.

Binding Constant Determination. Binding constants between Zn_2DPO and the chiral diamines are determined by a UV−visible spectroscopic titration method. The addition of PPDA (10^{-6} to 10^{-4} M) to the chloroform solution of Zn_2DPO (3.0×10^{-6} M) at room temperature primarily results in a red shift of the Soret (393 to 412 nm) and Q-bands (536 to 547, 571 to 581 nm). The nonlinear least-squares curve fitting of the absorption spectral data at 412 nm for 1:1 complexation was obtained by applying eq 1[19] in which A_0 and A_∞ are absorbances of Zn_2DPO and Zn_2DPO·PPDA, respectively, and [L] is the concentration of guest added.

$$A = (A_0 + K[\mathrm{L}]A_\infty)/(1 + K[\mathrm{L}]) \quad (1)$$

dx.doi.org/10.1021/ic401091r | Inorg. Chem. 2014, 53, 49−62

Absorbance A at 412 nm is then plotted against the concentration of ligand, [L], as demonstrated in Figure 16; K is found to be 1.50×10^5 M^{-1} from the nonlinear curve fitting.

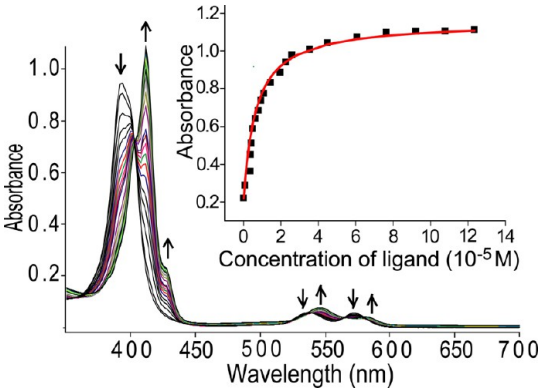

Figure 16. UV−visible spectral changes of Zn_2DPO in chloroform upon addition of (*S*)-PPDA as the host:guest molar ratio changes from 1:0 to 1:45 at 295 K. Inset shows the change of absorbance at 412 nm. Solid line represents the nonlinear least-squares for 1:1 complexation.

Similarly, binding constants between Zn_2DPO and diaminopropane are also determined. The addition of (*R*)-DAP (10^{-6} to 10^{-5} M) to the chloroform solution of Zn_2DPO (4.0×10^{-6} M) at room temperature also results in the red shift of the Soret (393 to 412 nm) and Q-bands (536 to 547, 571 to 581 nm). The nonlinear least-squares curve fitting of the spectral data at 412 nm for 1:1 complexation provides the binding constant (K) of 1.70×10^5 M^{-1}, as shown in Figure S8.

The binding constants of three other chiral diamines, CHDA, PEDA, and DPEA, with Zn_2DPO have also been estimated similarly and are found to be 1.60×10^5 M^{-1} (Figure S9), 4.80×10^4 M^{-1} (Figure S10), and 1.70×10^3 M^{-1} (Figure S11), respectively. It can be seen that the binding constant values follow the order DAP > CHDA > PPDA > PEDA, while the relatively bulkier ligand DPEA binds ∼100 times weaker compared to the DAP ligand as a result of steric interactions of two phenyl moieties in DPEA with the porphyrin rings. A smaller value of the binding constant with the PEDA guest ligand is also due to the presence of a bulky phenyl moiety.

Circular Dichroism (CD). CD has become a versatile tool for configuration assignment and the structural evaluation of the supramolecular complex. The interaction of the chiral diamine L with Zn_2DPO was monitored in solution using CD spectroscopy. Upon addition of increasing amounts of (*S*)-phenylpropanediamine (PPDA) to the chloroform solution of Zn_2DPO, the CD intensity gradually increases. The CD amplitude becomes maximal (A_{obs}, +419 M^{-1} cm^{-1}) upon addition of 30 equivalents of the chiral ligand. However, further addition of ligand up to 400 equivalents causes no change in CD intensity, which implies formation of a stable 1:1 sandwich complex; the spectral changes have been demonstrated in Figure 17. Thus, there is no evidence of formation of 1:2 host−guest complexes even at very high concentration of the guest ligand (which would result in a lowering of the CD intensity) because of the restricted rotation of the bisporphyrin ligand around the bridging O atom.[4] Similar behavior has also been observed with other diamine guest ligands reported here.

Figure 18 demonstrates CD and UV−vis spectra of all the complexes reported here, while Table 2 summarizes the spectral parameters observed for the complexes. A notably

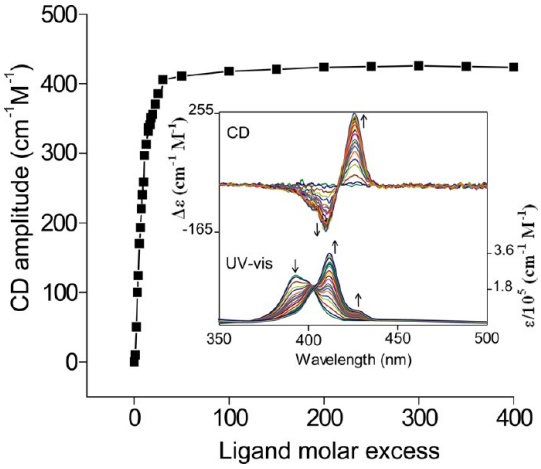

Figure 17. CD amplitude change upon addition of (*S*)-phenylpropanediamine to a chloroform solution of Zn_2DPO at 295 K as the host−guest molar ratio changes from 1:0 to 1:400. Inset shows the respective changes in CD and UV−visible spectra upon addition of guest ligand.

high magnitude CD signal (A_{obs}, −394 M^{-1} cm^{-1}) (Figure 18A) for Zn_2DPO·DAP can be ascribed to the complex's high stability (K = 1.70×10^5 M^{-1}) and formation of a unidirectional left-handed screw twisted by an angle of −33.4(5)° observed from the X-ray structure of the complex (*vide supra*). Preorganization of the diamine binding sites and pre-existing chirality therein would cause the two porphyrin macrocycles to be oriented in an anticlockwise direction in order to minimize host−guest steric interactions. The $-NH_2$ binding site of the *R*-stereocenter of the ligand is projected toward the Zn center (Figure 2) and hence becomes suitable to coordinate with minimal strain, while the other $-NH_2$ has no such preferential direction. Since there is no bulky substituent in the ligand for strong steric interaction with the porphyrin, the $-NH_2$ binding site can coordinate to the zinc center without any restriction. Thus, the direction of twist between the two porphyrin units is solely dictated by the projection of the $-NH_2$ group of the chiral center, i.e., the absolute configuration of the chiral center. On examination of the Corey−Pauling−Koltun (CPK) molecular model shown in Figure 19, it can be seen that the two porphyrin units are twisted in an anticlockwise direction to generate minimal host−guest repulsions. The interchromophoric anticlockwise twisting brings out a negative sign of the first Cotton effect of the CD couplet.

A remarkably high amplitude bisignate CD signal (A_{obs}, +515 M^{-1} cm^{-1}) (Figure 18B and Table 2) has been observed for Zn_2DPO·CHDA. Analysis of the X-ray structure of Zn_2DPO·CHDA reveals that two *trans*-oriented amino groups sitting above and below the chair form of the cyclohexane ring in CHDA are perfectly projected toward two Zn atoms of Zn_2DPO, leading to the formation of a 1:1 sandwich complex with high stability (K = 1.60×10^5 M^{-1}), which results in the formation of a unidirectional right-handed screw with torsion angles of +30.8(5)° and +30.9(5)° for molecules I and II, respectively. The CPK molecular model is shown in Figure 20A, which clearly demonstrates clockwise twisting of the two porphyrin units with minimum steric interaction between the bisporphyrin host and CHDA guest. Hence, the observation of the positive CD signal can be concluded from the interporphyrin clockwise twist. Similarly, Zn_2DPO·PPDA also

dx.doi.org/10.1021/ic401091r | *Inorg. Chem.* 2014, 53, 49−62

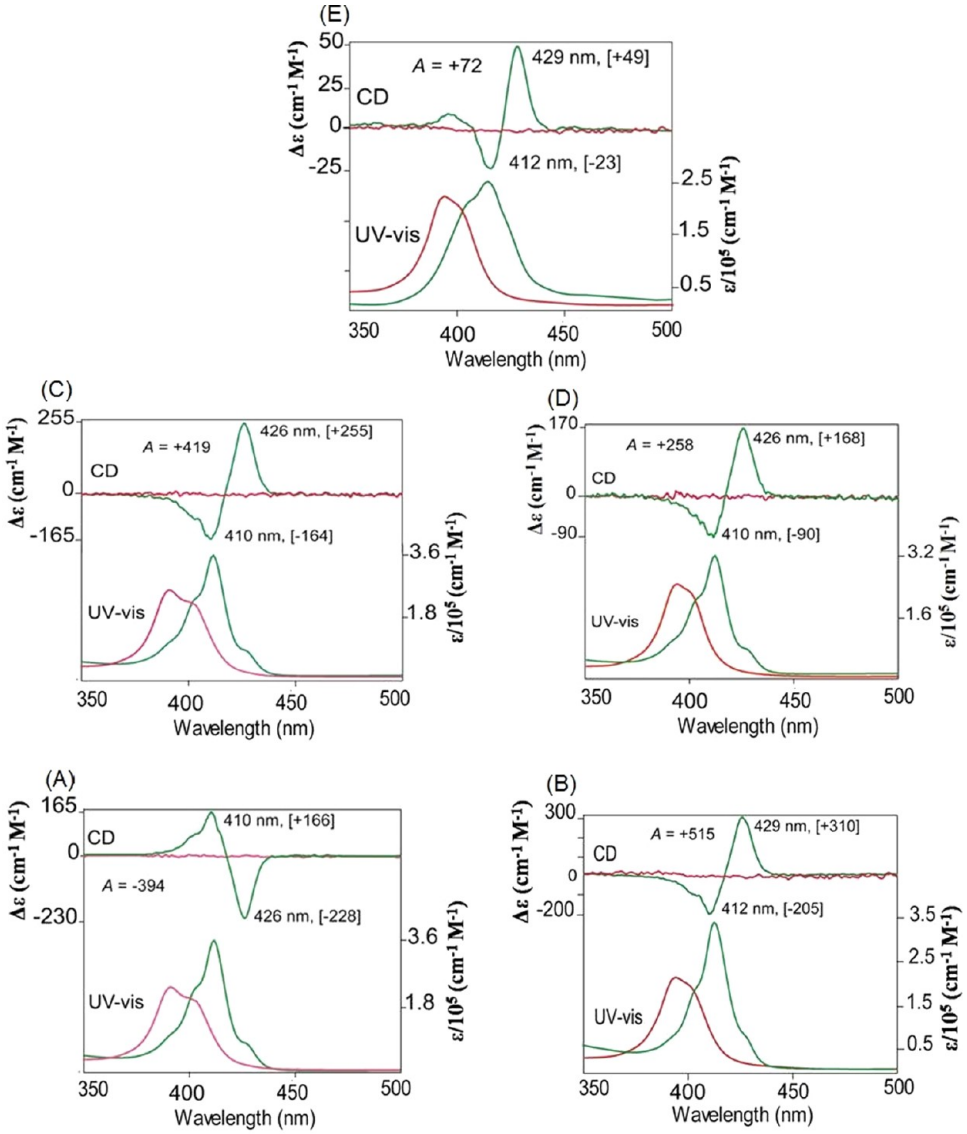

Figure 18. CD and UV−visible spectra (in $CHCl_3$ at 295 K) of Zn_2DPO, (A) in the absence (red) and the presence (green) of (*R*)-DAP, (B) in the absence (red) and the presence (green) of (1*S*,2*S*)-CHDA, (C) in the absence (red) and the presence (green) of (*S*)-PPDA, (D) in the absence (red) and the presence (green) of (*S*)-PEDA, and (E) in the absence (red) and the presence (green) of (1*R*,2*R*)-DPEA at their maximum concentration.

Table 2. UV−Vis and CD Spectral Data in Chloroform at 295 K

		CD data, λ (nm) [$\Delta\varepsilon$ (M^{-1} cm^{-1})]			
complex	UV−vis, λ (nm) B transitions	first Cotton	second Cotton	A_{obs}[a]	binding constant K (M^{-1})
Zn_2DPO·DAP	412, 426[sh]	426[−228]	410[+166]	−394	1.70×10^5
Zn_2DPO·CHDA	412, 429[sh]	429[+310]	412[−205]	+515	1.60×10^5
Zn_2DPO·PPDA	412, 426[sh]	426[+255]	410[−164]	+419	1.50×10^5
Zn_2DPO·PEDA	412, 426[sh]	426[+168]	410[−90]	+258	4.80×10^4
Zn_2DPO·DPEA	412, 429[sh]	429[+49]	412[−23]	+72	1.70×10^3

[a] A_{obs} (= $\Delta\varepsilon_1 - \Delta\varepsilon_2$) represents the total amplitude of the experimentally observed CD couplets.

shows high CD amplitude (A_{obs}, +419 M^{-1} cm^{-1}) (Figure 18C). Generation of such a highly intense CD couplet is attributed to the formation of the highly stable tweezer−diamine complex ($K = 1.50 \times 10^5$ M^{-1}) as well as unidirectional screw (torsional angle, +32.7(5)°) observed in the solid-state structure of the complex. The CPK model, depicted in Figure 20B, clearly shows a clockwise twisting of the two porphyrin units around the diphenyl ether bridge with minimum host−guest steric interactions for the complex. Zn_2DPO·PEDA also shows a positive CD signal (A_{obs}, +258 M^{-1} cm^{-1}) (Figure 18D) due to the clockwise twisting of the bisporphyrin moiety with a torsional angle of +35.2(5)°. The CPK molecular model, shown in Figure 20C, illustrates the clockwise orientation of the bisporphyrin with minimum host−guest steric strain. Thus for the complexes Zn_2DPO·CHDA, Zn_2DPO·PPDA, and Zn_2DPO·PEDA, two porphyrin macrocycles are twisted in a

dx.doi.org/10.1021/ic401091r | Inorg. Chem. 2014, 53, 49−62

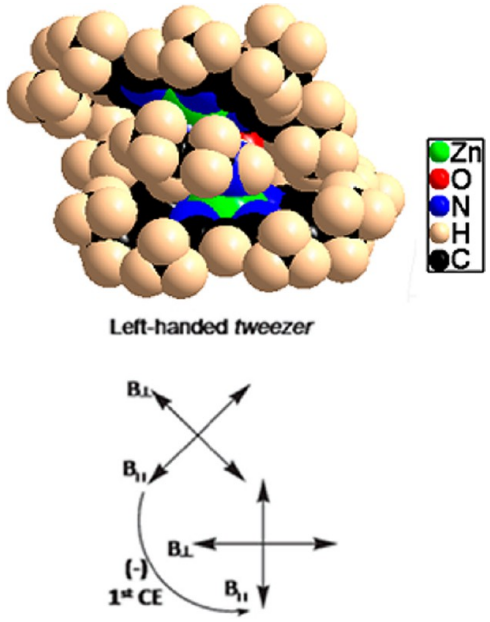

Figure 19. CPK molecular model of Zn_2DPO·DAP and corresponding coupling electronic transitions.

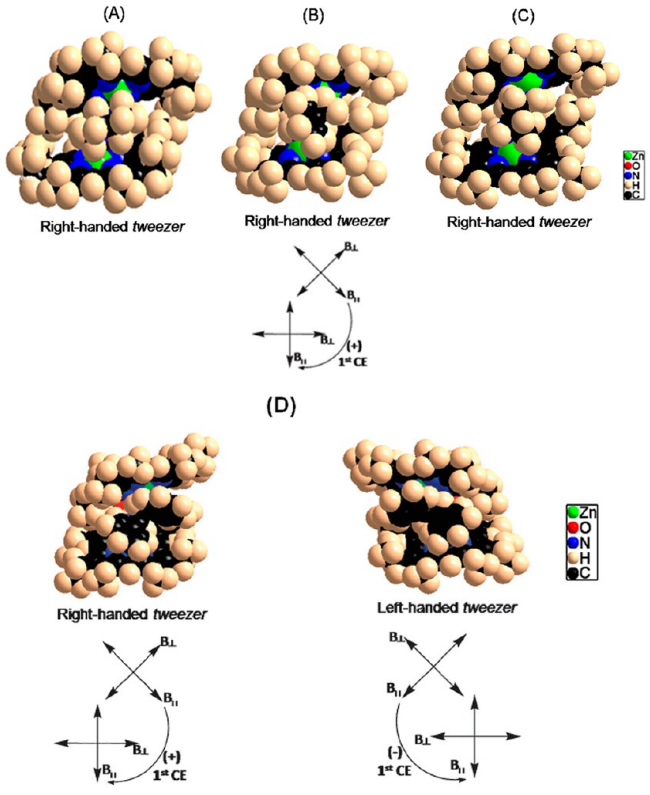

Figure 20. CPK molecular models of (A) Zn_2DPO·CHDA, (B) Zn_2DPO·PPDA, (C) Zn_2DPO·PEDA, and (D) Zn_2DPO·DPEA and corresponding coupling electronic transitions.

clockwise direction, for which a positive first Cotton effect in the CD couplet is observed. Thus, the above observations establish a firm correlation between the sign of the CD signal and the interporphyrin twist. Observation of a relatively lower CD amplitude of Zn_2DPO·PEDA compared to those of Zn_2DPO·DAP, Zn_2DPO·CHDA, and Zn_2DPO·PPDA is due to the lower binding constant value with PEDA. The more rigid nature of (1*S*,2*S*)-CHDA compared to (*R*)-DAP and (*S*)-PPDA may be responsible for the relatively large CD amplitude observed in Zn_2DPO·CHDA. However, the relatively higher CD amplitude was even observed when CHDA forms a 1:1 sandwich complex with ethane-bridged bis(zinc octaethylporphyrin) (A_{obs}, −590 M^{-1} cm^{-1}) as compared to Zn_2DPO (A_{obs}, +515 M^{-1} cm^{-1}). Such enhancement in CD intensity can be attributed to the highly flexible nature of ethane-bridged bisporphyrin, which produces a higher torsional angle of 54.1(5)° as compared to 30.9(5)° and 30.8(5)° observed for molecules I and II, respectively, in Zn_2DPO·CHDA.

In sharp contrast, Zn_2DPO·DPEA shows a very low amplitude bisignate positive CD signal (A_{obs}, +72 M^{-1} cm^{-1}) (Figure 18E and Table 2). Observation of such a low CD amplitude and, most notably, observation of a positive CD signal for the (*R*)-ligand is not "expected" according to the correlation obtained with other chiral diamines used in the present investigation. The presence of both right- and left-handed conformations of the complex, as observed in the X-ray crystal structure (Figure 10), contributes toward the intensity of the CD couplet in the opposite direction. The CPK model, shown in Figure 20D, demonstrates the presence of both molecules' twisted clockwise and anticlockwise orientation of the two porphyrin units with minimum host−guest steric interactions. The observations of a positive CD signal for Zn_2DPO·DPEA suggests that the right-handed structure is a greater contributor to the CD intensity than the left-handed one.

According to the pre-existing chirality of the (1*R*,2*R*)-DPEA, there could have been exclusively a unidirectional twist of left-handed screw sense; however, the right-handed molecule is also formed, as evident in the X-ray structure of Zn_2DPO·DPEA. Unlike other chiral ligands, DPEA has two bulky phenyl groups, which increases significantly steric repulsions in the host−guest complex, leading to the weaker binding of the ligand in Zn_2DPO·DPEA. A close observation of the X-ray structure of the left-handed molecule (Figure 21A) reveals that the bulky

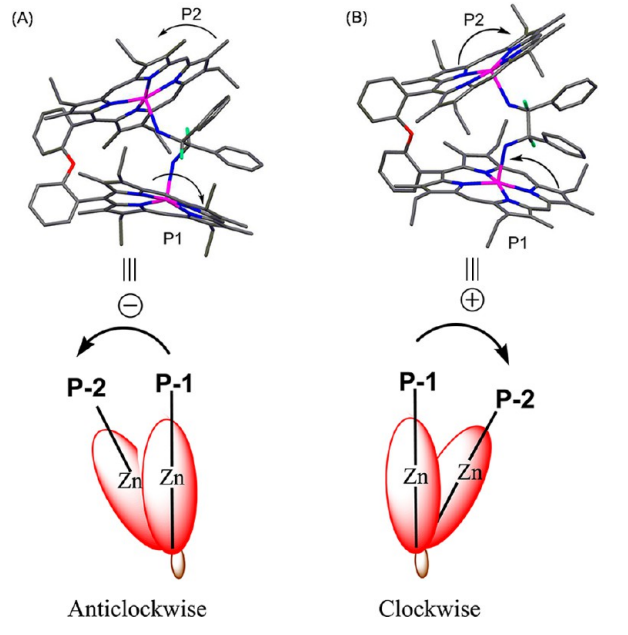

Figure 21. Binding mechanism between Zn_2DPO and (1*R*,2*R*)-DPEA resulting in (A) anticlockwise and (B) clockwise conformers.

dx.doi.org/10.1021/ic401091r | *Inorg. Chem.* 2014, 53, 49−62

phenyl substituent is *syn* to the porphyrin, which eventually generates large host−guest steric interactions, leading to a longer Zn−N_{ax} distance of 2.232(8) Å. In order to avoid the steric interaction caused by the two phenyl moieties, the two porphyrin units also undergo a clockwise twisting in which the bulky phenyl group can be placed *anti* to the porphyrin ring (Figure 21B), leading to a relatively shorter Zn−N_{ax} distance of 2.209(8) Å, which is also evident in the X-ray structure of the complex.

From the X-ray structure of Zn_2DPO·DPEA, it is observed that there are two factors that control the direction of interporphyrin twist of the complex. The preorganized projection of the NH_2 group of the chiral center in (1*R*,2*R*)-DPEA dictates anticlockwise twist between two porphyrin units (Figure 21A) which leads to negative sign of the first Cotton effect of the CD couplet. However, steric differentiation would lead clockwise twisting of two porphyrin rings (Figure 21B) which provide positive sign of the first Cotton effect of the CD couplet. From the observed positive CD signal of the complex, it can be concluded that the right-handed structure has relatively greater contribution to the CD amplitude than the left-handed one. Hence, Zn_2DPO·DPEA shows a postive CD signal although the intensity is very low. It is important to note that two molecules are also present in the asymmetric unit of Zn_2DPO·CHDA (Figure 4) but both of them shows large clockwise twist between the two porphyrin units that are solely dictated by the projection of the -NH_2 group of the (1*S*,2*S*)-chiral center since no bulky substituent are present in CHDA for significant steric interactions. As a result, the complex shows a remarkably high amplitude bisignate CD signal (A_{obs}, +515 M^{-1} cm^{-1}). It can be concluded that the spatial orientation of the two porphyrin rings, and hence the sign of the CD couplet in the Soret region, is essentially dependent upon the projection of the ligand's functional groups, size of the ligand's substituent and the host−guest interactions.

CONCLUSIONS

Synthesis, X-ray structure and properties of supramolecular tweezer-diamine complexes Zn_2DPO·DAP, Zn_2DPO·CHDA, Zn_2DPO·PPDA, Zn_2DPO·PEDA, and Zn_2DPO·DPEA have been demonstrated here. All these complexes consist of achiral Zn(II) bisporhyrin (Zn_2DPO) host and enantiomerically pure chiral diamines, namely, (*R*)-DAP, (1*S*,2*S*)-CHDA, (*S*)-PPDA, (*S*)-PEDA, and (1*R*,2*R*)-DPEA as guest ligands, respectively. ^{1}H NMR of the host−guest complex reveals large upfield shift of the guest protons due to the ring current effect of the bisporphyrin tweezer. Largest upfield shift that is observed for the N*H*$_2$ protons of the guest ligand follow the order Zn_2DPO·DAP > Zn_2DPO·CHDA > Zn_2DPO·PPDA> Zn_2DPO·PEDA ≫ Zn_2DPO·DPEA which happens to be the order of binding constant of the respective chiral diamine with Zn_2DPO. While other tweezer−diamine complexes showed well-resolved ^{1}H NMR signals, Zn_2DPO·DPEA depicts very broad resonances.

As the bulk of the substituent at the stereogenic center of the diamine guest increases, the Zn−N_{ax} distance in the tweezer−diamine complex also increases which eventually lowers the binding of guest ligand toward the host. While in four 1:1 sandwich complexes, a large unidirectional screw has been observed in the bisporphyrin moiety around the diphenylether bridge, only in Zn_2DPO·DPEA, two molecules with very different structure and geometrical parameters are observed due to the presence of two bulky phenyl substituents in the DPEA guest ligand. In one, the two zinc porphyrins are twisted in a clockwise direction while they rotate in an anticlockwise direction in the other one. Two molecules are also present in the asymmetric unit of Zn_2DPO·CHDA, however, both of them have similar structural and geometrical parameters with large clockwise twist between two porphyrin units.

Upon formation of a tweezer−diamine complex between an achiral Zn_2DPO host and a chiral diamine guest, a bisignate CD signal arises in the porphyrin Soret band region. The pre-existing chirality of the diamine guests would make the two porphyrin macrocycles to be oriented in a clockwise/anticlockwise direction in order to minimize host−guest steric interaction. Notably high amplitude bisignate CD signal responded by Zn_2DPO·DAP, Zn_2DPO·CHDA, and Zn_2DPO·PPDA can be ascribed to the complex's high stability and formation of unidirectional screw as observed from the X-ray structures. Relatively lower CD amplitude has been observed for Zn_2DPO·PEDA because of the lower binding affinity of PEDA due to the presence of a bulky phenyl moiety at the stereocenter. It has been observed that (*S*)-guest shows positive CD couplet while (*R*)-guest produces negative CD couplet as dictated by the pre-existing chirality of (*R*)-DAP, (1*S*,2*S*)-CHDA, (*S*)-PPDA, and (*S*)-PEDA ligands.

In sharp contrast, Zn_2DPO·DPEA shows a very low amplitude bisignate positive CD signal (A_{obs}, +72 M^{-1} cm^{-1}) and also have very low binding affinity. Observation of such low CD amplitude and the most significantly, observation of positive CD signal for (*R*)-ligand is contrary to the "expected" negative CD signal. The projection of the −NH_2 group in (1*R*,2*R*)-DPEA (in which bulky phenyl group is *syn* to the porphyrin ring) dictates an anticlockwise twist of the two porphyrin units, leading to a negative sign of the first Cotton effect of the CD couplet. However, steric differentiation (in which the bulky phenyl group is *anti* to the porphyrin ring) also forced the two porphyrin units to be twisted in a clockwise orientation, which, however, provides a positive sign of the first Cotton effect of the CD couplet. The resultant weak positive CD signal expressed by the Zn_2DPO·DPEA comes from the contribution of the clockwise twisted molecule surpassing the contribution of the anticlockwise twisted one. In Zn_2DPO·CHDA, however, both of the molecules show a large clockwise twist of the two porphyrin units that is solely dictated by the projection of the −NH_2 group of the *S*-chiral center due to lack of significant steric clash within the host−guest complex. As a result, the complex shows a remarkably high amplitude bisignate CD signal (A_{obs}, +515 M^{-1} cm^{-1}). Thus, the spatial orientation of the two porphyrin rings is essentially dependent upon the projection of the ligand's binding functional groups attached to the stereocenter as well as the steric differentiation at the chiral center. Binding affinity of the chiral guest ligand and the flexibility of the bisporphyrin architecture are also responsible for the CD signal intensity. The present work thus demonstrates a full and unambiguous rationalization of the observed chirality transfer processes from the chiral guest to the achiral host that is observed in many natural and artificial supramolecular assemblies.

EXPERIMENTAL SECTION

Materials. The synthesis of 4,6-bis[Zn(II) 5-(3,7,13,17-tetraethyl-2,6,12,16-tetramethylporphyrinyl)]diphenyl ether, Zn_2DPO, was accomplished using the literature methods.[17] Reagents and solvents were purchased from commercial sources and purified by standard procedures before use. Enantiomerically pure (*S*)-3-phenylpropane-1,2-diamine, (*S*)-PPDA, and (*S*)-phenylethylenediamine, (*S*)-PEDA,

dx.doi.org/10.1021/ic401091r | *Inorg. Chem.* 2014, 53, 49−62

have been synthesized by following the procedure reported in the literature.[20]

Syntheses of Zn_2DPO·DAP. To a solution of Zn(II) bisporphyrin, Zn_2DPO (50 mg, 0.039 mmol), in distilled dichloromethane (2.5 mL) was added (*R*)-diaminopropane (3.5 mg, 0.047 mmol), and the mixture was stirred for 10−12 min. The solution, thus obtained, was then filtered off to remove any solid residue and carefully layered with *n*-hexanes. On standing for 6−7 days in air at room temperature, dark crystalline solids were precipitated out, which were then isolated by filtration, washed well with *n*-hexanes, and dried well under vacuum. Yield: 42 mg (79%). Anal. Calcd (found): C, 71.64 (71.55); H, 6.70 (6.80); N, 10.58 (10.67). UV−vis (chloroform) [λ_{max}, nm (ε, M^{-1} cm^{-1})]: 412 (3.62×10^5), 426^{sh} (7.78×10^4), 547 (2.60×10^4), 581 (1.36×10^4). ^{1}H NMR ($CDCl_3$, 295 K): δ 9.84 (br, 2H, 10-*meso*-*H*); 9.41 (s, 2H, 15-*meso*-*H*); 8.77 (s, 2H, 20-*meso*-*H*); 8.48 (br, 2H, Ar-*H*); 7.89 (br, 2H, Ar-*H*); 7.35 (br, 2H, Ar-*H*); 6.97 (br, 2H, Ar-*H*); 3.97−2.90 (m, 16H, $-CH_2$); 1.87−1.25 (m, 48H, $-CH_3$); −4.63 (m, 3H, $-CH_3$, DAP); −5.56 (m, 1H, H^1, DAP); −6.53 (m, 1H, H^3, DAP); −6.63 (m, 1H, H^2, DAP); −8.10 (br, 2H, $-NH_2$); −8.22 (br, 2H, $-NH_2$) ppm.

Zn_2DPO·CHDA. Zn(II) bisporphyrin, Zn_2DPO (50 mg, 0.039 mmol), was dissolved in 2.5 mL of distilled chloroform. (1*S*,2*S*)-CHDA (5.4 mg, 0.047 mmol) was added to it and stirred for 10−12 min. The resulting solution was then filtered off to remove any solid residue and carefully layered with *n*-hexanes. On standing for 6−7 days in air at room temperature, dark crystalline solids were precipitated out, which were then collected by filtration, washed well with *n*-hexanes, and dried well under vacuum. Yield: 45 mg (82%). Anal. Calcd (found): C, 72.32 (72.23); H, 6.81 (6.92); N, 10.29 (10.38). UV−vis (chloroform) [λ_{max}, nm (ε, M^{-1} cm^{-1})]: 412 (3.45×10^5), 429^{sh} (7.87×10^4), 546 (2.45×10^4), 580 (1.39×10^4). ^{1}H NMR ($CDCl_3$, 295 K): δ 10.04 (s, 2H, 10-*meso*-*H*); 9.83 (s, 2H, 15-*meso*-*H*); 9.43 (s, 2H, 20-*meso*-*H*); 8.58 (d, 1H, Ar-*H*); 8.16 (d, 1H, Ar-*H*); 7.96 (t, 1H, Ar-*H*); 7.92 (t, 1H, Ar-*H*); 7.76 (t, 1H, Ar-*H*); 7.15 (t, 1H, Ar-*H*); 7.08 (d, 1H, Ar-*H*); 6.99 (d, 1H, Ar-*H*); 3.96−2.93 (m, 16H, $-CH_2$); 1.85−1.04 (m, 48H, $-CH_3$); −0.75 (m, 2H, H^1, CHDA); −2.33 (m, 2H, H^2, CHDA); −3.50 (m, 2H, H^3, CHDA); −6.42 (m, 2H, H^4, CHDA); −7.05 (m, 2H, H^5, CHDA); −7.91 (m, 4H, $-NH_2$).

Zn_2DPO·PPDA. Zn(II) bisporphyrin, Zn_2DPO (50 mg, 0.039 mmol) was dissolved in 2.5 mL of distilled dichloromethane, and (*S*)-PPDA (7.1 mg, 0.047 mmol) was added to the solution, which was stirred at room temperature for 10−12 min. The resulting solution was filtered to remove any solid residue and then carefully layered with acetonitrile and kept for slow diffusion at room temperature in air. On standing for 6−7 days, a dark crystalline solid of the molecule was formed, which was then collected by filtration, washed well with acetonitrile, and dried well under vacuum. Yield: 43 mg (77%). Anal. Calcd (found): C, 72.90 (72.82); H, 6.62 (6.71); N, 10.00 (10.12). UV−vis (chloroform) [λ_{max}, nm (ε, M^{-1} cm^{-1})]: 412 (3.58×10^5), 426^{sh} (7.75×10^4), 547 (2.58×10^4), 581 (1.36×10^4). ^{1}H NMR ($CDCl_3$, 295 K): δ 9.87 (s, 1H, 10-*meso*-*H*); 9.80 (s, 1H, 10-*meso*-*H*); 9.53 (s, 1H, 15-*meso*-*H*); 9.39 (s, 1H, 15-*meso*-*H*); 8.84 (s, 1H, 20-*meso*-*H*); 8.69 (s, 1H, 20-*meso*-*H*); 8.53 (d, 2H, Ar-*H*); 7.89 (m, 2H, Ar-*H*); 7.34 (br, 2H, Ar-*H*); 7.19 (br, 2H, Ar-*H*); 6.87 (m, 1H, −C*H*, PPDA); 6.81 (*m*, 2H, −C*H*, PPDA); 4.32 (br, 2H, −C*H*, PPDA); 4.09−2.91 (m, 16H, $-CH_2$); 1.87−1.19 (m, 48H, $-CH_3$); −3.06 (br, 1H, H^4, PPDA); −3.85 (br, 1H, H^5, PPDA); −5.21 (br, 1H, H^1, PPDA); −5.74 (br, 1H, H^3, PPDA); −6.36 (br, 1H, H^2, PPDA); −7.55 (br, 2H, $-NH_2$); −7.87 (br, 2H, $-NH_2$) ppm.

Zn_2DPO·PEDA. Zn(II) bisporphyrin, Zn_2DPO (50 mg, 0.039 mmol), was dissolved in 2.5 mL of distilled dichloromethane, and (*S*)-PEDA (6.4 mg, 0.047 mmol) was added to the solution, which was stirred at room temperature for 15 min. The solution was filtered to remove any solid residue and slowly layered with acetonitrile. After allowing to stand for 6−7 days, a dark crystalline solid were precipitated out, which was filtered, washed with acetonitrile, and dried well under vacuum. Yield: 42 mg (76%). Anal. Calcd (found): C, 72.77 (72.71); H, 6.54 (6.59); N, 10.10 (10.18). UV−vis (chloroform) [λ_{max}, nm (ε, M^{-1} cm^{-1})]: 412 (3.22×10^5), 426^{sh} (7.71×10^4), 547 (2.55×10^4), 581 (1.32×10^4). ^{1}H NMR ($CDCl_3$, 295 K): δ 9.85 (s, 2H, 10-*meso*-*H*); 9.50 (br, 2H, 15-*meso*-*H*); 9.00 (s, 2H, 20-*meso*-*H*); 8.52 (br, 2H, Ar-*H*); 7.90 (br, 4H, Ar-*H*); 7.08 (br, 2H, Ar-*H*); 6.39 (br, 1H, −C*H*, PEDA); 6.03 (br, 2H, −C*H*, PEDA); 3.92−3.02 (m, 18H, −C*H*, PEDA, $-CH_2$); 2.11−1.26 (m, 48H, $-CH_3$); −4.97 (br, 1H, H^1); −5.57 (br, 1H, H^3); −6.28 (br, 1H, H^2); −6.78 (br, 2H, $-NH_2$); −7.48 (br, 2H, $-NH_2$) ppm.

Zn_2DPO·DPEA. Zn(II) bisporphyrin, Zn_2DPO (50 mg, 0.039 mmol), was dissolved in 2.5 mL of distilled chloroform. (1*R*,2*R*)-DPEA (9.9 mg, 0.047 mmol) was added to it and stirred for nearly 15 min. The resulting solution was then filtered off to remove any solid residue and carefully layered with *n*-hexanes. On standing for 6−7 days in air at room temperature, a dark crystalline solid of the molecule was formed, which was then collected by filtration, washed well with cyclohexane, and dried well under vacuum. Yield: 44 mg (75%). Anal. Calcd (found): C, 74.04 (74.15); H, 6.49 (6.55); N, 9.60 (9.69) UV−vis (chloroform) [λ_{max}, nm (ε, M^{-1} cm^{-1})]: 412 (2.47×10^5), 429^{sh} (5.39×10^4), 543 (2.44×10^4), 577 (1.77×10^4). ^{1}H NMR ($CDCl_3$, 218 K): 10.07 (s, 2H, 10-*meso*-*H*); 10.03 (s, 2H, 15-*meso*-*H*); 10.01 (s, 2H, 20-*meso*-*H*); 8.05 (d, 1H, Ar-*H*); 7.81 (d, 1H, Ar-*H*); 7.69 (m, 2H, Ar-*H*); 7.29 (d, 2H, Ar-*H*); 7.07 (t, 1H, Ar-*H*); 6.91 (br, 1H, Ar-*H*); 6.74 (m, 2H, −C*H*, DPEA); 6.60 (m, 4H, −C*H*, DPEA); 5.31 (m, 4H, −C*H*, DPEA); 4.08−3.61 (m, 16H, $-CH_2$); 2.69−0.80 (m, 48H, $-CH_3$); −0.62 (br, 2H, −C*H*, DPEA); −1.60 (br, 4H, $-NH_2$, DPEA).

Instrumentation. UV−visible and circular dichroism spectra were recorded on a PerkinElmer UV/vis spectrometer and JASCO J-815 spectrometer, respectively. Elemental (C, H, and N) analyses were performed on a CE-440 elemental analyzer. ^{1}H NMR spectra were recorded on a JEOL 500 MHz instrument. The residual ^{1}H resonances of the solvents were used as a secondary reference.

X-ray Structure Solution and Refinement. Crystals were coated with light hydrocarbon oil and mounted in the 100 K dinitrogen stream of a Bruker SMART APEX CCD diffractometer equipped with a CRYO Industries low-temperature apparatus, and intensity data were collected using graphite-monochromated Mo Kα radiation (λ = 0.71073 Å). The data integration and reduction were processed with SAINT software.[21] An absorption correction was applied.[22] Structures were solved by the direct method using SHELXS-97 and were refined on F^2 by a full-matrix least-squares technique using the SHELXL-97 program package.[23] Non-hydrogen atoms were refined anisotropically. In the refinement, hydrogens were treated as riding atoms using SHELXL default parameters. In the structure of Zn_2DPO·DAP, two badly disordered CH_2Cl_2 were present, which could not be modeled successfully and, therefore, SQUEEZE[24] was used. Crystal data and data collection parameters are shown in Table S2.

■ ASSOCIATED CONTENT

Ⓢ Supporting Information

Job's plots (Figure S1), diagrams highlighting the bulk of the chiral guest ligands within the bisporphyrin envelope (Figure S2), ^{1}H NMR (Figures S3 and S4), ^{1}H−^{1}H COSY (Figures S5−S7), UV−visible spectral change and binding constant determination (Figures S8−S11), selected bond distances (Å) and bond angles (deg) for the complexes (Table S1), and crystal data and data collection parameters (Table S2). X-ray crystallographic details in CIF format. This material is available free of charge via the Internet at http://pubs.acs.org.

■ AUTHOR INFORMATION

Corresponding Author

*E-mail: sprath@iitk.ac.in. Tel: (+91)-512-259-7251. Fax: (+91)-512-259-7436.

Notes

The authors declare no competing financial interest.

dx.doi.org/10.1021/ic401091r | *Inorg. Chem.* 2014, 53, 49−62

■ ACKNOWLEDGMENTS

The authors thank the Department of Science and Technology, Government of India, and CSIR, New Delhi, for financial support. S.B. and S.A.I. thank CSIR, India, for the fellowship.

■ DEDICATION

Dedicated to Professor R. N. Mukherjee on the occassion of his 60th birthday.

■ REFERENCES

(1) (a) Ito, H.; Tsukube, H.; Shinoda, S. *Chem. Commun.* **2012**, *48*, 10954. (b) Ye, Y.; Chang, S.-W. *Appl. Phys. Lett.* **2012**, *101*, 181106. (c) Davis, A. P.; Wareham, R. S. *J. Am. Chem. Soc.* **2010**, *132*, 16753. (d) Li, Y.; Wang, T.; Liu, M. *Soft Matter* **2007**, *3*, 1312. (e) Yashima, E.; Maeda, K.; Okamoto, Y. *Nature* **1999**, *399*, 449.

(2) (a) Schwartz, E.; Gac, S. L.; Cornelissen, J. L. M. J.; Nolte, R. J. M.; Rowan, A. E. *Chem. Soc. Rev.* **2010**, *39*, 1576. (b) Berova, N.; Pescitelli, G.; Petrovica, A. G.; Proni, G. *Chem. Commun.* **2009**, 5958. (c) Hembury, G. A.; Borovkov, V. V.; Inoue, Y. *Chem. Rev.* **2008**, *108*, 1. (d) Berova, N.; Bari, L. D.; Pescitelli, G. *Chem. Soc. Rev.* **2007**, *36*, 914. (e) Borovkov, V. V.; Hembury, G. A.; Inoue, Y. *Acc. Chem. Res.* **2004**, *37*, 449. (f) Huang, X.; Nakanishi, K.; Berova, N. *Chirality* **2000**, *12*, 237.

(3) (a) Borovkov, V. V.; Fujii, I.; Muranaka, A.; Hembury, G. A.; Tanaka, T.; Ceulemans, A.; Kobayashi, N.; Inoue, Y. *Angew. Chem., Int. Ed.* **2004**, *43*, 5481. (b) Borovkov, V. V.; Lintuluoto, J. M.; Hembury, G. A.; Sugiura, M.; Arakawa, R.; Inoue, Y. *J. Org. Chem.* **2003**, *68*, 7176. (c) Borovkov, V. V.; Lintuluoto, J. M.; Inoue, Y. *Org. Lett.* **2002**, *4*, 169. (d) Borovkov, V. V.; Lintuluoto, J. M.; Sugeta, H.; Fujiki, M.; Arakawa, R.; Inoue, Y. *J. Am. Chem. Soc.* **2002**, *124*, 2993. (e) Borovkov, V. V.; Lintuluoto, J. M.; Sugiura, M.; Inoue, Y.; Kuroda, R. *J. Am. Chem. Soc.* **2002**, *124*, 11282. (f) Lintuluoto, J. M.; Borovkov, V. V.; Inoue, Y. *J. Am. Chem. Soc.* **2002**, *124*, 13676. (g) Borovkov, V. V.; Lintuluoto, J. M.; Inoue, Y. *J. Am. Chem. Soc.* **2001**, *123*, 2979. (h) Borovkov, V. V.; Yamamoto, N.; Lintuluoto, J. M.; Tanaka, T.; Inoue, Y. *Chirality* **2001**, *13*, 329.

(4) Brahma, S.; Ikbal, S. A.; Dey, S.; Rath, S. P. *Chem. Commun.* **2012**, *48*, 4070.

(5) (a) Chaudhary, A.; Ikbal, S. A.; Brahma, S.; Rath, S. P. *Polyhedron* **2013**, *52*, 761. (b) Brahma, S.; Ikbal, S. A.; Rath, S. P. *Inorg. Chim. Acta* **2011**, *372*, 62.

(6) (a) Petrovic, A. G.; Vantomme, G.; Abril, Y. L. N.; Lubian, E.; Saielli, G.; Menegazzo, I.; Cordero, R.; Proni, G.; Nakanishi, K.; Carofiglio, T.; Berova, N. *Chirality* **2011**, *23*, 808. (b) Chen, Y.; Petrovic, A. G.; Roje, M.; Pescitelli, G.; Kayser, M. M.; Yang, Y.; Berova, N.; Proni, G. *Chirality* **2010**, *22*, 140. (c) Petrovic, A. G.; Chen, Y.; Pescitelli, G.; Berova, N.; Proni, G. *Chirality* **2010**, *22*, 129. (d) Pescitelli, G.; Gabriel, S.; Wang, Y.; Fleischhauer, J.; Woody, R. W.; Berova, N. *J. Am. Chem. Soc.* **2003**, *125*, 7613. (e) Proni, G.; Pescitelli, G.; Huang, X.; Nakanishi, K.; Berova, N. *J. Am. Chem. Soc.* **2003**, *125*, 12914. (f) Proni, G.; Pescitelli, G.; Huang, X. F.; Quraishi, N. Q.; Nakanishi, K.; Berova, N. *Chem. Commun.* **2002**, 1590. (g) Huang, X.; Fujioka, N.; Pescitelli, G.; Koehn, F. E.; Williamson, R. T.; Nakanishi, K.; Berova, N. *J. Am. Chem. Soc.* **2002**, *124*, 10320. (h) Kurtàn, T.; Nesnas, N.; Li, Y.-Q.; Huang, X.; Nakanishi, K.; Berova, N. *J. Am. Chem. Soc.* **2001**, *123*, 5962. (i) Kurtàn, T.; Nesnas, N.; Koehn, F. E.; Li, Y.-Q.; Nakanishi, K.; Berova, N. *J. Am. Chem. Soc.* **2001**, *123*, 5974. (j) Huang, X. F.; Borhan, B.; Rickman, B. H.; Nakanishi, K.; Berova, N. *Chem.—Eur. J.* **2000**, *6*, 216.

(7) (a) Tanasova, M.; Borhan, B. *Eur. J. Org. Chem.* **2012**, 3261. (b) Li, X.; Burrell, C. E.; Staples, R. J.; Borhan, B. *J. Am. Chem. Soc.* **2012**, *134*, 9026. (c) Tanasova, M.; Vasileiou, C.; Olumolade, O. O.; Borhan, B. *Chirality* **2009**, *21*, 374. (d) Li, X.; Borhan, B. *J. Am. Chem. Soc.* **2008**, *130*, 16126. (e) Li, X.; Tanasova, M.; Vasileiou, C.; Borhan, B. *J. Am. Chem. Soc.* **2008**, *130*, 1885. (f) Yang, Q.; Olmsted, C.; Borhan, B. *Org. Lett.* **2002**, *4*, 3423.

(8) (a) Pintre, I. C.; Pierrefixe, S.; Hamilton, A.; Valderrey, V.; Bo, C.; Ballester, P. *Inorg. Chem.* **2012**, *51*, 4620. (b) Etxebarria, J.; Ferran, A. V.; Ballester, P. *Chem. Commun.* **2008**, 5939.

(9) (a) Kai, H.; Nara, S.; Kinbara, K.; Aida, T. *J. Am. Chem. Soc.* **2008**, *130*, 6725. (b) Muraoka, T.; Kinbara, K.; Aida, T. *Nature* **2006**, *440*, 23. (c) Mizuno, Y.; Alam, M. A.; Tsuda, A.; Kinbara, K.; Yamaguchi, K.; Aida, T. *Angew. Chem., Int. Ed.* **2006**, *45*, 3786. (d) Guo, Y.-M.; Oike, H.; Saeki, N.; Aida, T. *Angew. Chem., Int. Ed.* **2004**, *43*, 4915. (e) Mizuno, Y.; Aida, T. *Chem. Commun.* **2003**, 20.

(10) (a) Hayashi, T.; Aya, T.; Nonoguchi, M.; Mizutani, T.; Hisaeda, Y.; Kitagawa, S.; Ogoshi, H. *Tetrahedron* **2002**, *58*, 2803. (b) Ogoshi, H.; Mizutani, T. *Acc. Chem. Res.* **1998**, *31*, 81. (c) Hayashi, T.; Nonoguchi, M.; Aya, T.; Ogoshi, H. *Tetrahedron Lett.* **1997**, *38*, 1603.

(11) (a) D'Urso, A.; Nicotra, P. F.; Centonze, G.; Fragalá, M. E.; Gattuso, G.; Notti, A.; Pappalardo, A.; Pappalardo, S.; Parisi, M. F.; Purrello, R. *Chem. Commun.* **2012**, *48*, 4046. (b) D'Urso, A.; Fragalá, M. E.; Purrello, R. *Chem. Commun.* **2012**, *48*, 8165.

(12) (a) Yoon, H.; Lee, C.-H.; Jang, W.-D. *Chem.—Eur. J.* **2012**, *18*, 12479. (b) Bringmann, G.; Götz, D. C. G.; Gulder, T. A. M.; Gehrke, T. H.; Bruhn, T.; Kupfer, T.; Radacki, K.; Braunschweig, H.; Heckmann, A.; Lambert, C. *J. Am. Chem. Soc.* **2008**, *130*, 17812. (c) Hou, J. L.; Yi, H.-P.; Shao, X.-B.; Li, C.; Wu, Z.-Q.; Jiang, X.-K.; Wu, L.-Z.; Tung, C.-H.; Li, Z.-T. *Angew. Chem., Int. Ed.* **2006**, *45*, 796. (d) Kimura, M.; Kitamura, T.; Sano, M.; Muto, T.; Hanabusa, K.; Shirai, H.; Kobayashi, N. *New J. Chem.* **2000**, *24*, 113. (e) Monti, D.; Cantonetti, V.; Venanzi, M.; Ceccacci, F.; Bombelli, C.; Mancini, G. *Chem. Commun.* **2004**, 972.

(13) (a) Ishii, Y.; Yoshizawa, T.; Kubo, Y. *Org. Biomol. Chem.* **2007**, *5*, 1210. (b) Ishii, Y.; Onda, Y.; Kubo, Y. *Tetrahedron Lett.* **2006**, *47*, 8221.

(14) (a) Crossley, M. J.; Mackay, L. G.; Try, A. C. *J. Chem. Soc., Chem. Commun.* **1995**, 1925. (b) Crossley, M. J.; Hambley, T. W.; Mackay, L. G.; Try, A. C.; Walton, R. *J. Chem. Soc., Chem. Commun.* **1995**, 1077.

(15) (a) Ouyang, Q.; Zhu, Y. Z.; Li, Y. C.; Wei, H. B.; Zheng, J. Y. *J. Org. Chem.* **2009**, *74*, 3164. (b) Ema, T.; Nemugaki, S.; Tsuboi, S.; Utaka, M. *Tetrahedron Lett.* **1995**, *36*, 5905. (c) Holmes, A. E.; Das, D.; Canary, J. W. *J. Am. Chem. Soc.* **2007**, *129*, 1506.

(16) (a) Liu, G.; Wang, F.; Chaunchaiyakul, S.; Saito, Y.; Bauri, A. K.; Kimura, T.; Kuwahara, Y.; Komatsu, N. *J. Am. Chem. Soc.* **2013**, *135*, 4805. (b) Veling, N.; van Hameren, R.; van Buul, A. M.; Rowan, A. E.; Nolte, R. J. M.; Elemans, J. A. A. W. *Chem. Commun.* **2012**, *48*, 4371. (c) Yoon, H.; Lee, C. H.; Jang, W. D. *Chem.—Eur. J.* **2012**, *18*, 12479. (d) Webb, S. J.; Sanders, J. K. M. *Inorg. Chem.* **2000**, *39*, 5920.

(17) Gros, C. P.; Brisach, F.; Meristoudi, A.; Espinosa, E.; Guilard, R.; Harvey, P. D. *Inorg. Chem.* **2007**, *46*, 125.

(18) Kasha, M.; Rawls, H. R.; Bayoumi, M. A. E. *Pure Appl. Chem.* **1965**, *11*, 371.

(19) Fukuzumi, S.; Kondo, Y.; Mochizuki, S.; Tanaka, T. *J. Chem. Soc., Perkin Trans. 2* **1989**, 1753.

(20) Belokon, Y. N.; Pritula, L. K.; Tararov, V. I.; Bakhmutov, V. I.; Struchkov, Y. T.; Timofeeva, T. V.; Belikov, V. M. *J. Chem. Soc., Dalton Trans.* **1990**, 1867.

(21) *SAINT+*, 6.02 ed.; Bruker AXS: Madison, WI, 1999.

(22) Sheldrick, G. M. *SADABS 2.0*; 2000.

(23) Sheldrick, G. M. *Acta Crystallogr., Sect. A* **2008**, *64*, 112.

(24) Spek, A. L. *J. Appl. Crystallogr.* **2003**, *36*, 7.